Draft version January 2, 2017
Typeset using LaTeX **twocolumn** style in AASTeX61

OPTIFCAL OBSERVATIONS OF AN EXTRAORDINARILY YOUNG TYPE IA SUPERNOVA IPTF16ABC

Yi Cao[1] and Friends[2]

[1] *eScience Institute and Astronomy Department, University of Washington, Seattle, WA 98195*
[2] *the intermediate Palomar Transient Factory*

(Received January 2, 2017; Revised January 2, 2017; Accepted January 2, 2017)

Submitted to ApJ

ABSTRACT

In this paper, we present observations of a young normal Type Ia supernova iPTF16abc. Our analysis shows that: blabla ...

Keywords: methods: observational — supernovae: individual (iPTF16abc)

Corresponding author: Yi Cao
ycao16@uw.edu

1. INTRODUCTION

Although Type Ia supernovae (SNe Ia) have been extensively used as standardizable candles, their progenitor scenarios and explosion physics are still in debate (see a recent review by Maoz et al. 2014). Detailed extremely early-phase observations are one of the most promising avenues to further constrain this problem.

While the shock breakout of a SN Ia occurs on a sub-second timescale, the subsequent quasi-adiabatic expanding and cooling of the unbinded ejecta produces thermal emissions that can be used to infer the original size of the exploding star (Piro et al. 2010; Rabinak & Waxman 2011). Comparing models of these cooling emissions to the earliest-phase data of SN2011fe, Bloom et al. (2012) concluded that the radius of the progenitor star is $\lesssim 0.01 R_\odot$ where $R_\odot$ is the solar radius. Combining this size constraint and the measured ejecta mass to derive the mean density of the progenitor star, we confirmed that the progenitor star is compact and degenerate. Admittedly, due to the initial small surface area of the progenitor star, the shock cooling emission of a SN Ia decays drastically as the ejecta expands. Given typical parameters of a SN Ia, this thermal emission is visible from events up to ~ 10 Mpc within one day of their explosions.

Another expectation from the extremely early-phase observations of a SN Ia is the excess emission from collisions between SN ejecta and a companion star, a natural consequence from the single-degenerate progenitor hypothesis (Whelan & Iben 1973; Kasen 2010). In a low-velocity SN Ia iPTF14atg, Cao et al. (2015) for the first time detected a strong and declining ultraviolet pulse within a few days of the SN explosion which is best interpreted as the SN-companion collision. This signature has been searched in a number of nearby, early-phase normal SNe Ia, but most of these studies result in no detection (Hayden et al. 2010; Bianco et al. 2011; Foley et al. 2012; Bloom et al. 2012; Olling et al. 2015; Zheng et al. 2013; Goobar et al. 2015; Shappee et al. 2016b; Im et al. 2015). The exception is SN2012cg which Marion et al. (2016) claimed detection of blue excess in the earliest-phase light curve and attribute it to SN-companion collision. However, this statement is recently challenged by Shappee et al. (2016a). In fact, it is not surprising that no SN-companion collision has been observationally confirmed, because only up to $\sim 10\%$ of events from the single-degenerate channel have the preferred binary geometry for us to see the collision signatures.

More commonly, the only observed light curve of a SN Ia is purely powered by the radioactive decay of synthesized ^{56}Ni. Since ^{56}Ni atoms are synthesized, mixed and deposited into different layers inside the ejecta, the SN may experience a dark period after the SN shock breakout and before the radioactive energy diffuses to the photosphere (Piro & Nakar 2014). In the case of strong mixing, ^{56}Ni energy can reach the photosphere rapidly. As such, the dark period is very short and the light curve shows a fast initial rise. In the opposite case, it may take up to a couple of days for the ^{56}Ni energy to diffuse to the photosphere. The initial rise of the light curve is then moderate (Piro & Morozova 2016). To summarize, the initial rise of the light curve of a SN Ia conveys information on distribution of synthesized ^{56}Ni.

In this paper, we report observations of an extraordinarily young SN Ia iPTF16abc, which was discovered by the intermediate Palomar Transient Factory on 2016 April 3.36[1] at R.A. $= 13^h34^m45.49^s$, Dec. $= +13^d51^m14.3^s$ (J2000) with a g-band magnitude of 21.31 ± 0.27 (Cao et al. 2016; Miller et al. 2016). The transient is spatially coincident with a tidal tail of the galaxy NGC 5221 at 100 Mpc. No activity was detected at the same location down to $g = 22.1$ mag on April 2.42. Our spectroscopic follow-up compaign classified iPTF16abc as a normal SN Ia (Cenko et al. 2016).

This paper is organized as follows: Section 2 describes photometric and spectroscopic observations of iPTF16abc. Section 3 establishes that iPTF16abc is a normal SN Ia in NGC 5221. Section 4 analyzes the early light curve and spectra.

2. OBSERVATIONS

ycao: TODO: include LCOGT data in both text and figures.

As part of the iPTF transient survey in the 2016 spring quarter, the field of iPTF16abc was observed in g- or R-band every night by the CFH12K camera (Starr et al. 2000) on the 48-inch telescope at Palomar Observatory (P48). The images were processed by the IPAC image subtraction and discovery pipeline which subtracts off the background galaxy light with stacked pre-SN images and performs forced point-spread-function (PSF) photometry at the location of the SN. The photometry is then calibrated to the PTF photometric catalog (Ofek et al. 2012).

After discovery, we utilized the rainbow camera of the SED Machine (ycao: REF) mounted on the 60-inch telescope at Palomar Observatory (P60) to undertake photometric observations in g, r and i filters. The image differencing against the archival SDSS images and forced PSF photometry on the subtracted images were

[1] all times in this paper are in UTC.

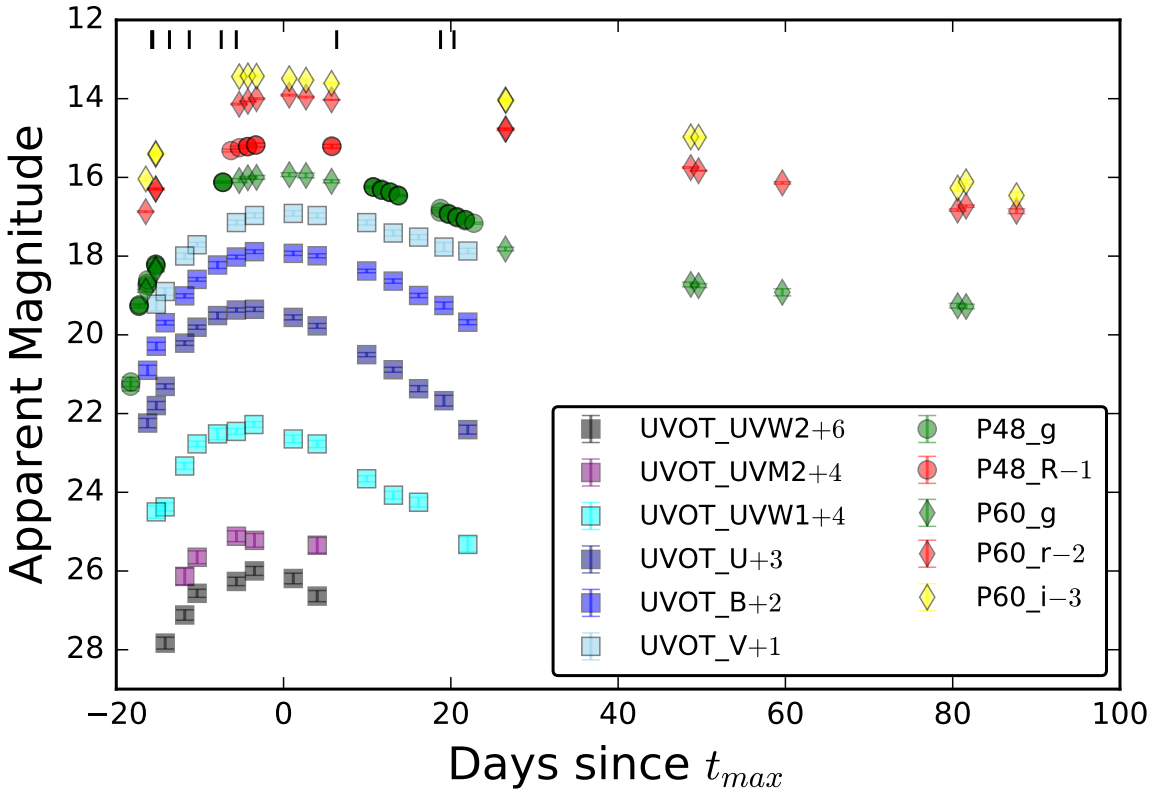

Figure 1. Multi-band light curves of iPTF16abc are shown. Filters are denoted by different colors and observation instruments by different markers. The t_{max} time is the B-band maximum determined by SALT2 (Section). The black ticks near the top of the figure shows epochs of spectroscopic observations.

performed by the Fremling Automated Pipeline (Fremling et al. 2016). The photometry is also calibrated to the SDSS catalog.

Las Cambres Observatory Global Network (LCOGT) also carry out photometric observations in the *BVgri* filters with its 1-m telescope network. ycao: Some info about data reduction

In space, *Swift* observed iPTF16abc for 14 epochs, covering from the very early phase to the post-peak phase. Aperture photometry are carried out on the images taken by its Ultraviolet-Optical Telescope (UVOT) with the usual procedures in the HEASoft and corrected for the coincident loss and aperture loss. No pre-SN UVOT image at the SN location is available in the *Swift* archive. Visual inspection to the UVOT images suggests that the background galaxy light in the UVOT filters is probably negligible. No X-ray emission was detected at the location of the SN by the X-ray Telescope (XRT) in any of these for epochs.

The multi-color light curves of iPTF16abc are illustrated in Figure 1. For convenience, all magnitudes are in the AB system with a zero point of 3631 Jy in all filters.

Spectroscopic observations of iPTF16abc were undertaken with the Gemini Multi-Object Spectrograph (GMOS; Hook et al. 2004) on the Gemini North telescope, Low-Resolution Imaging Spectrometer (LRIS; Oke et al. 1995) on the Keck-I telescope, DEep Imaging Multi-Object Spectrograph (DEIMOS; Faber et al. 2003) on the Keck-II telescope, The Andalucia Faint Object Spectrograph and Camera (ALFOSC[2]) on the Nordic Optical Telescope (NOT), and X-shooter (Vernet et al. 2011) and Ultraviolet and Visual Echelle Spectrograph (UVES; Dekker et al. 2000) on the Very Large Telescope (VLT). The observing log is listed in Table 1 and the low-resolution spectral sequence is shown in Figure 2.

3. REDDENING, CLASSIFICATION AND HOST GALAXY

3.1. *Reddening*

[2] ALFOSC instrument webpage: http://www.not.iac.es/instruments/alfosc/

Table 1. Spectroscopic observations of iPTF16abc

Observation Date	SN phase	Telescope/Instrument	Exposure Time (s)	Wavelength Coverage (Å)	Resolution
2016 April 05.88	−15.8	Gemini-North/GMOS		3500 – 9500	1900
2016 April 06.51	−15.1	Keck-II/DEIMOS	1491	5500 – 8100	2000
2016 April 08.51	−13.1	Keck-II/DEIMOS	900	5500 – 8100	2000
2016 April 10.38	−11.3	Keck-I/LRIS	300	3000 – 10000	1000
2016 April 14.20	−7.5	VLT/XSHOOTER		3000 – 25000	10000
2016 April 16.??	−5.?	VLT/UVES		covers Ca II H+K and Na I D lines	40000
2016 April 28.??	6.4	NOT/ALFOSC		3300 – 9000	360
2016 May 10.42	18.8	Keck-I/LRIS	600	3000 – 10000	1000
2016 May 12.03	20.4	VLT/XSHOOTER		3000 – 25000	10000

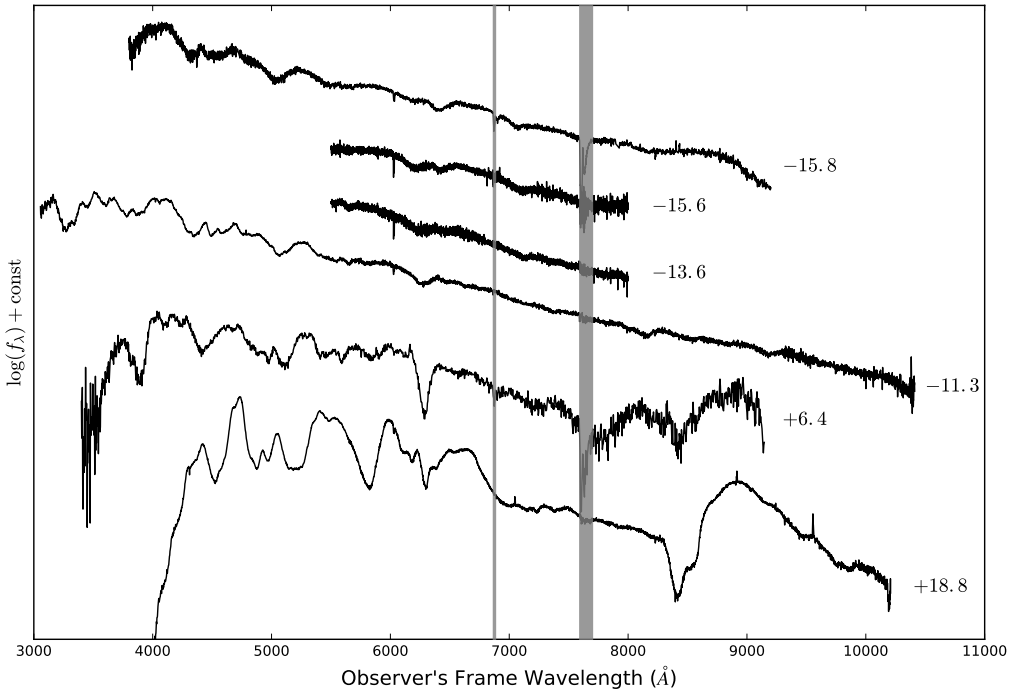

Figure 2. Low-resolution spectra of iPTF16abc are shown in the chronical sequence. The phases in units of days are labeled next to corresponding spectra. Telluric absorption bands are grayed out.

The foreground Galactic extinctioin along the directionof iPTF16abc has $E(B-V) = 0.0279$ mag (Schlafly & Finkbeiner 2011).

In the highest-resolution spectrum of iPTF16abc by UVES, individual components of both Ca II H+K and Na I D doublets show double-absorption profiles (Figure 3), indicating two sources of absorption along the line of sight. Fitting two Gaussian kernels to each line of the Na I doublet simultaneously leads to redshifts of $0.02313820 \pm 0.00000032$ and $0.02322408 \pm 0.00000033$. The total equivalent widths of the Na I D1 and D2 lines are 0.595 ± 0.009 Å and 0.609 ± 0.008 Åm, respectively.

Using the empirical relation between the equivalent width of Na I D lines and reddening $E(B-V)$ (Poznanski et al. 2012), we derive $E(B-V) = 0.361 \pm 0.025$mag.

In the X-shooter spectra of iPTF16abc, we also identify narrow absorption features K I 7665 Åand 7699 Åat consistent redshifts. However, the resolution of the X-shooter spectra is not fine enough to resolve the double-absorption profiles of Ca II and Na I. The X-shooter spectra do not show the diffusive interstellar band at 5780 Åas well. Albeit some debates (e.g., Phillips et al. 2013), the $E(B-V)$ value derived from Na I D absorption provides the best estimate in the case of iPTF16abc.

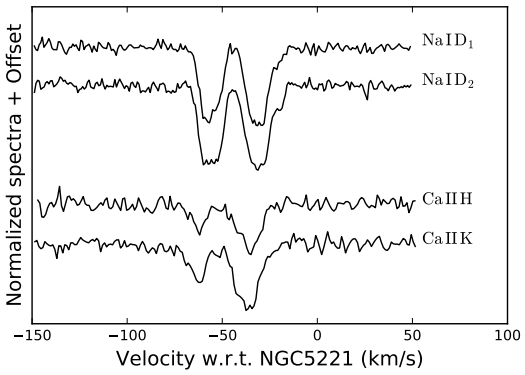

Figure 3. Narrow absorption lines of iPTF16abc are shown in this figure. The zero velocity corresponds to the redshift of the apparent host NGC 5221.

The Na I D doublet are seen in multiple spectra spanning from pre-peak to post-peak phases. Despite the instrumental widening of different instrument configurations, we do not detect obvious variation in the profiles of the doublet.

3.2. *Classfication*

We run Supernova Identification (SNID; Blondin & Tonry 2007) on the low-resolution spectrum of iPTF16abc at +18.8 and found best matches to normal SNe Ia. In fact, the characteristic features of a SN Ia, such as Si II, S II, can be easily identified in the spectra of iPTF16abc (Figure 2).

Next we standardize the light curve of iPTF16abc by feeding its P48 and P60 light curves into the `sncosmo` module[3] and fit a light curve model, which composes of the SALT2 template (Guy et al. 2007) modified by the line-of-sight extinction curve (Fitzpatrick 1999) with $E(B-V)$ values from Section 3.1 and $R_V = 3.1$. We obtain the rest-frame B-band peak time $\mathrm{MJD}_{max} = 57499.65 \pm 0.02$, the coefficient of the zeroth principle component $x_0 = 0.0275 \pm 0.0002$, the coefficient of the first principle component $x_1 = 1.200 \pm 0.043$, and the color term $c = -0.3353 \pm 0.0054$. The best-fit model also gives an unreddened apparent peak magnitude of $m_B^* = 14.4$ mag in the SN rest frame.

For convenience, in the following sections, we define the best-fit value $\mathrm{MJD}_{max} = 57499.65$ as phase $t = 0$.

[3] The `sncosmo` Python module is available at `https://sncosmo.readthedocs.io/en/v1.4.x/`.

3.3. *Host Galaxy*

After establishing iPTF16abc as a normal SN ia, we use the latest calibration (Betoule et al. 2014) of the Phillips relation (Phillips 1993) using m_B^*, x_1 and c to derive a distance modulus $\mu = 34.66 \pm 0.03$ mag to the SN, provided that the host galaxy of iPTF16abc has a stellar mass less than $10^{10} M_\odot$.

The location of iPTF16abc is spatially coincident with a tidal tail of galaxy NGC 5221. Theureau et al. (2007) derived a distance modulus of 35.0 ± 0.4 mag from the Tully-Fisher relation. This distance modulus is consistent with that of iPTF16abc.

Separately, Theureau et al. (1998) observed the 21-cm line in this galaxy and measured a redshift of 0.0233303 ± 0.000027. The two components in the Na I D have a relative velocity of $-57.6 \pm 8.1\,\mathrm{km\,s^{-1}}$ and $-31.8 \pm 8.1\,\mathrm{km\,s^{-1}}$, suggesting that both absorption resources are probaly located on the tidal tail of NGC 5221.

4. FIRST LIGHT AND EXPLOSION TIME

In this section, we estimate the first light and explosion time of iPTF16abc.

4.1. *Light Curve Fit*

Extrapolation of the earliest-phase light curve with a simple model is usually used to estimate the first light time. In theory, Arnett (1982) derived a quadratic law for an expanding fireball with a constant temperature. In order to account for the temperature change, here we utilize a power-law model

$$f(t) \begin{cases} = 0, \text{ when } t < t_0 \\ \propto (t - t_0)^\alpha, \text{ when } t > t_0 \end{cases} . \quad (1)$$

Since the first few detections of the SN were made in the g band, we perform the fit only to the g-band light curve. We experiment the fitting procedure with different time windows and find that the SN flux between $t = -19$ days and $t = -15$ days rises approximately linearly. The joint distribution of α and t_0 for this time window is given in the left panel of Figure 4 and the best fit model with

$\alpha = 0.94$ and $t_0 = -18.47$ is shown in the right panel. With this best-fit value of t_0, our first observation was made only 0.18 day after the first light of the SN. The total rise time to the B-band peak is 18.47 days.

Since $t = -15$ days, the g-band light curve rises significantly faster than the best-fit model above, indicating a greater value of the power-law index α. In fact, the light curve between $t = -14$ and $t = -8$ days can be fitted with a power law of index 1.40.

A more sophisticated broken power-law model has also been used to fit SN early-phase light curves (e.g., Zheng et al. 2013, 2014; Zheng & Filippenko 2016,?). Our above result has indicates that the g-band light curve of iPTF16abc can also be fitted by a broken-power law with a power index changing from 0.94 to 1.40. In fact, many young SNe, including SN2011fe Zheng & Filippenko (2016) and iPTF16abc, have early light curves that follow broken power-laws (Zheng et al. 2016)). Our above result has indicates that the g-band light curve of iPTF16abc can also be fitted by a broken-power law with a power index changing from 0.94 to 1.40.

The initial rise of a SN depends on the distribution of ^{56}Ni in the ejecta. Comparing the rapid initial rise of iPTF16abc to theoretical calculations in Piro & Morozova (2016) suggests strong mixing of ^{56}Ni in the iPTF16abc ejecta. The radioactive energy from ^{56}Ni can quickly diffuse to the SN photosphere and power its light curve after the SN explosion.

4.2. *Expansion Velocity Fit*

The first light of a SN is not necessarily its explotion time t_{exp}. Thanks to different deposition of ^{56}Ni in the SN ejecta, as pointed out in Piro & Nakar (2014), the SN may experience a dark period before the radioactive energy from the shallowest ^{56}Ni layer escapes the ejecta. Therefore, Piro & Nakar (2014) suggests to examine evolution of absorption line velocities, because the velocities do not depend on the ^{56}Ni mixing and are expected to evolve roughly as $v \propto (t - t_{exp})^{-0.22}$.

We focus on measuring velocities of the strongest Si II 6355 line, as the second most commonly used Ca II IR triplet is very weak in iPTF16abc. Visual inspection of the early-phase spectra shows no sign of any high-velocity component of the Si II line and that the red wing of Si II overlaps the C II 6580 line. Therefore, we fit simultaneously two gaussian kernels for the two lines and a linear term to account for the continuum component. Then the velocities are calculated at the minimum of the Si II gaussian kernel.

Fitting the measured velocities of Si II 6355 line to the $v \propto (t - t_{exp})^{-0.22}$ model leads to the best-fit explosion time $t_{exp} = -17.95$ days with a 3-σ confidence interval between -17.4 days and -18.3 days (Figure 5). We further test the robustness of a fixed power-law index by altering the index to -0.20 and -0.24 and find consistent results within respective 3-σ confidence intervals.

The derived t_{exp} is roughly consistent to t_0 estimated in Section 4.1, confirming that the dark period of iPTF16abc is very short. This conclusion is consistent with the inference from the rapid initial rise of iPTF16abc in Section 4.1.

Among the several SNe with measurements of t_{exp} and t_0 (Piro & Nakar 2014; Shappee et al. 2016b), iPTF16abc has the shortest dark period and longest rise time (18.47 days). In comparison, SN2011fe is inferred to have a dark period of ~ 1 day (Piro & Nakar 2014) and a rise time of 17.7 days (Pereira et al. 2013); ASASSN-14lp has a dark period of a couple of days and a rise time of 16.94 days. This seems to suggest that the time difference between SN explosion and the B-band maximum, which equals to summation of the dark period and the rise time, is a constant for a SN Ia. This is perhaps because the B-band maximum time only depends on the total amount of ^{56}Ni.

4.3. *Strong and Short-Lived Carbon Features*

Interestingly, the first few spectra of iPTF16abc show clear detection of C II 6580 and C II 7234 lines. Their velocity evolution is shown in Figure 5 as well.

The C II lines only appear in the very early phases. The equivalent widths of detected C II 6580 and C II 7234 lines are shown in Figure 6, and are compared to that of the Si II 6355 line. Especially in the first spectrum taken at $t = -15.8$ days, the C II equivalent widths are stronger than that of Si II.

The strong and short-lived C II features suggest that the outermost layers of the ejecta contain a certain amount of carbon which is responsible for the C II absorption. The abundance of carbon drops dramatically into the inner layers of the ejecta.

Carbon signatures are seen in over 1/4 of all normal SNe Ia before maxima (Parrent et al. 2011; Silverman & Filippenko 2012; Thomas et al. 2011), but the signatures are usually weak. Even in SN2011fe, the C II features are not strong in the first spectra (Parrent et al. 2012). The only normal SN Ia known to have strong C II features at very early phases is SN2013dy (Zheng et al. 2013). Unlike iPTF16abc, the equivalent widths of C II features in SN2013dy are as large as that of Si II 6355.

4.4. *Discussions and Physical Constraints*

The early radiation of a SN Ia may have multiple resources: SN shockbreakout, SN-companion collision, and radioactive activity. Since each provides interesting

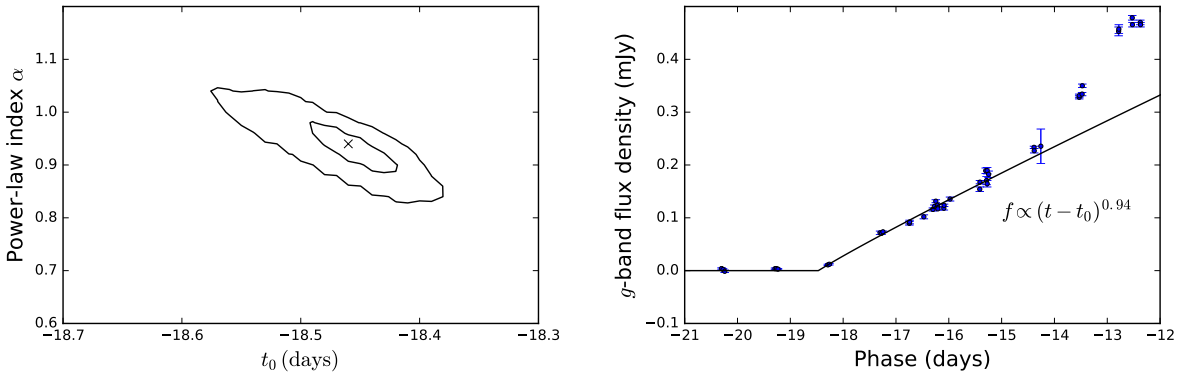

Figure 4. Broken Power low fitting to the early g-band light curve. *Left:* the joint distribution of t_0 and α. The cross marker denotes the best-fit parameters. The inner and outer contours represent the 68% and 99.7% confidence levels. *Right:* the best-fit model of $\alpha = 0.94$ and $t_0 = -18.47$ days is illustrated against the data.

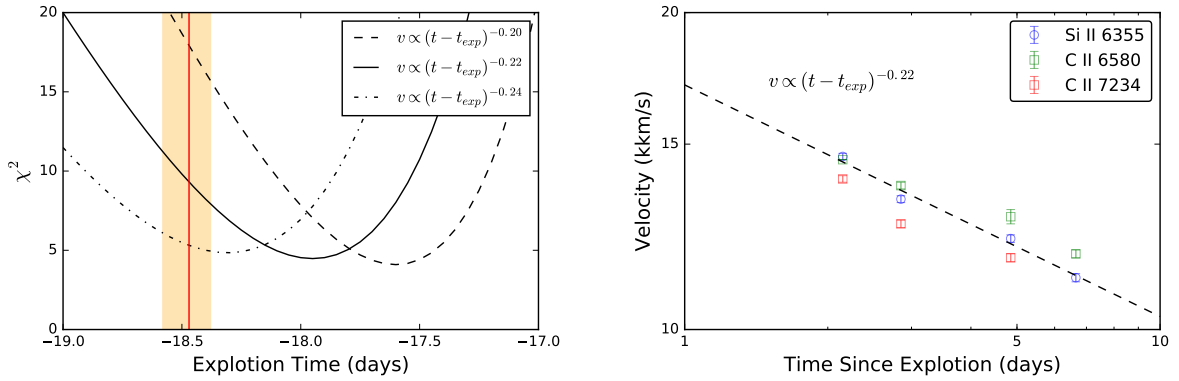

Figure 5. Constraints on t_{exp} from fitting the velocity evolution of Si II. *Left panel:* the dashed, solid and dash-dotted curves show χ^2 for fitting power laws with indices -0.20, -0.22 and -0.24, respectively. The red vertical line and the orange region indicate t_0 and its 3-σ confidence interval from Section 4.1. *Right panel:* Observed Si II 6355 velocities with the best-fit power-law velocity with an index of -0.22.

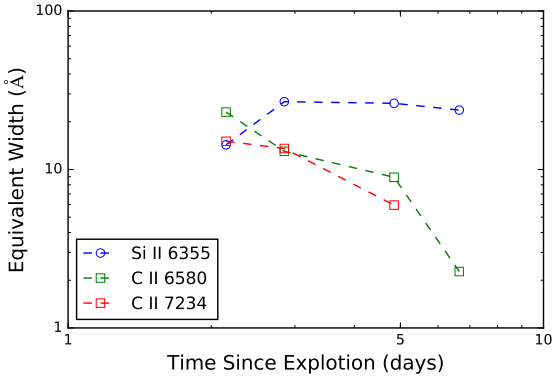

Figure 6. Equivalent Width of Si II 6355, C II 6580 and C II 7234 lines

constraints on the progenitor properties, we explore all the three posibilities.

4.4.1. *SN Shock Breakout*

The shock breakout of a SN Ia lasts for a fraction of a second due to the small size of the exploding star. However, the subsequent cooling phase may last longer (e.g., Piro et al. 2010). Following the analysis of SN2011fe in Bloom et al. (2012), we compare the early-phase g-band light curve of iPTF16abc with two cooling models (Rabinak & Waxman 2011; Piro et al. 2010) and reach a not very constraining conclusion that the radius of the progenitor star of iPTF16abc should be $< 1R_{\odot}$. In fact, the cooling emission is negligible at the time of the first detection of iPTF16abc.

4.4.2. *SN companion*

If iPTF16abc is born in a single-degenerate channel, with an odd of $\lesssim 10\%$, we expect to see emission produced by SN ejecta slamming into the companion. However, according to calculations by Kasen (2010), collision between SN ejecta and the companion star produces

thermal emission with a spectrum that peaks in the ultraviolet, and the Rayleigh-Jeans tail emission in the g band is very weak.

In the case of SN2012cg, in order to illustrate a blue excess in the early light curve, Marion et al. (2016) fitted a power-law model to its light curves between $t = -14$ days and $t = -8$ days and subtracted the extrapolated fluxes at early epochs. Then these authors attribute the excess to SN-companion collision. In our iPTF16abc, we follow the same procedure and also find a similar excess (Figure 7).

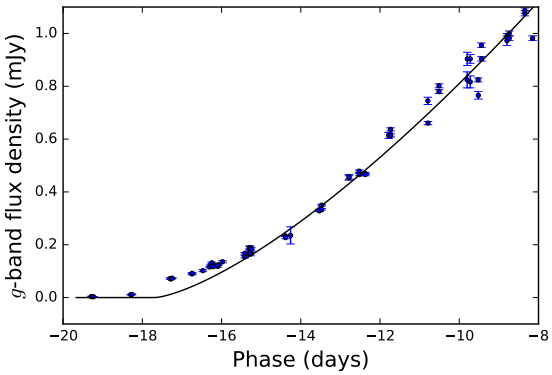

Figure 7. The early-phase g-band light curve of iPTF16abc is compared against the best-fit power-law model to the data segment between $t = -14$ and $t = -8$ days. Note the "excess" between the data and the model during $t = -18$ and $t = -15$ days

Actually, for any early light curve that can be approximated by a broken power law, as long as the asymptotic power-law index near $t = 0$ is less than that at late time, one can always find such an excess near $t = 0$. There are not many SNe that were observed at extraordinarily early phases. The odd that both SN2012cg and iPTF16abc show SN-companion collision signautres is very small.

Separately, our first *Swift* observation of iPTF16abc was made about two days after explosion. However, the ultraviolet light curve of iPTF16abc does not show any excess.

4.4.3. *Explosion Mechanism*

Our extraordinarily early observations of iPTF16abc put two constraints on the mechanism of the SN explosion: first, during the SN explosion, synthesized ^{56}Ni should be strongly mixed in the ejecta; second, unburned carbon atoms are accelerated to very high velocities in the ejecta. In addition, the commonly seen Ca II IR triplet is weak in iPTF16abc, implying a little amount of calsium in the ejecta.

5. CONCLUSION

In this paper, we present observations of a normal Type Ia supernova iPTF16abc, which is located at one tidal tail of NGC 5221. Our extraordinarily early-phase optical observations of this supernova show that:

- Extrapolation of the early light curve shows that our first observation was made only 0.18 days after the first light of the SN.
- The rapid initial rise and analysis of the line velocity both shows that the dark period of iPTF16abc is very short. Hence, the first light time of the SN is a good approximation to the time of the SN explosion.
- Strong and short-lived carbon features in the early spectra of iPTF16abc indicates concentration of unburned carbon in the fastest-moving part of the ejecta.

REFERENCES

Arnett, W. D. 1982, ApJ, 253, 785

Betoule, M., Kessler, R., Guy, J., et al. 2014, A&A, 568, A22

Bianco, F. B., Howell, D. A., Sullivan, M., et al. 2011, ApJ, 741, 20

Blondin, S., & Tonry, J. L. 2007, ApJ, 666, 1024

Bloom, J. S., Kasen, D., Shen, K. J., et al. 2012, ApJL, 744, L17

Cao, Y., Nugent, P. E., & Kasliwal, M. M. 2016, PASP, 128, 114502

Cao, Y., Kulkarni, S. R., Howell, D. A., et al. 2015, Nature, 521, 328

Cenko, S. B., Cao, Y., Kasliwal, M., et al. 2016, The Astronomer's Telegram, 8909

Dekker, H., D'Odorico, S., Kaufer, A., Delabre, B., & Kotzlowski, H. 2000, in Proc. SPIE, Vol. 4008, Optical and IR Telescope Instrumentation and Detectors, ed. M. Iye & A. F. Moorwood, 534–545

Faber, S. M., Phillips, A. C., Kibrick, R. I., et al. 2003, in Proc. SPIE, Vol. 4841, Instrument Design and Performance for Optical/Infrared Ground-based Telescopes, ed. M. Iye & A. F. M. Moorwood, 1657–1669
Fitzpatrick, E. L. 1999, PASP, 111, 63
Foley, R. J., Challis, P. J., Filippenko, A. V., et al. 2012, ApJ, 744, 38
Fremling, C., Sollerman, J., Taddia, F., et al. 2016, A&A, 593, A68
Goobar, A., Kromer, M., Siverd, R., et al. 2015, ApJ, 799, 106
Guy, J., Astier, P., Baumont, S., et al. 2007, A&A, 466, 11
Hayden, B. T., Garnavich, P. M., Kasen, D., et al. 2010, ApJ, 722, 1691
Hook, I. M., Jørgensen, I., Allington-Smith, J. R., et al. 2004, PASP, 116, 425
Im, M., Choi, C., Yoon, S.-C., et al. 2015, ApJS, 221, 22
Kasen, D. 2010, ApJ, 708, 1025
Maoz, D., Mannucci, F., & Nelemans, G. 2014, ARA&A, 52, 107
Marion, G. H., Brown, P. J., Vinkó, J., et al. 2016, ApJ, 820, 92
Miller, A. A., Laher, R., Masci, F., et al. 2016, The Astronomer's Telegram, 8907
Ofek, E. O., Laher, R., Surace, J., et al. 2012, PASP, 124, 854
Oke, J. B., Cohen, J. G., Carr, M., et al. 1995, PASP, 107, 375
Olling, R. P., Mushotzky, R., Shaya, E. J., et al. 2015, Nature, 521, 332
Parrent, J. T., Thomas, R. C., Fesen, R. A., et al. 2011, ApJ, 732, 30
Parrent, J. T., Howell, D. A., Friesen, B., et al. 2012, ApJL, 752, L26
Pereira, R., Thomas, R. C., Aldering, G., et al. 2013, A&A, 554, A27
Phillips, M. M. 1993, ApJL, 413, L105
Phillips, M. M., Simon, J. D., Morrell, N., et al. 2013, ApJ, 779, 38
Piro, A. L., Chang, P., & Weinberg, N. N. 2010, ApJ, 708, 598
Piro, A. L., & Morozova, V. S. 2016, ApJ, 826, 96
Piro, A. L., & Nakar, E. 2014, ApJ, 784, 85
Poznanski, D., Prochaska, J. X., & Bloom, J. S. 2012, MNRAS, 426, 1465
Rabinak, I., & Waxman, E. 2011, ApJ, 728, 63
Schlafly, E. F., & Finkbeiner, D. P. 2011, ApJ, 737, 103
Shappee, B. J., Piro, A. L., Stanek, K. Z., et al. 2016a, ArXiv e-prints, arXiv:1610.07601
Shappee, B. J., Piro, A. L., Holoien, T. W.-S., et al. 2016b, ApJ, 826, 144
Silverman, J. M., & Filippenko, A. V. 2012, MNRAS, 425, 1917
Starr, B. M., Luppino, G. A., Cuillandre, J.-C., & Isani, S. 2000, in Proc. SPIE, Vol. 3965, Sensors and Camera Systems for Scientific, Industrial, and Digital Photography Applications, ed. M. M. Blouke, N. Sampat, G. M. Williams, & T. Yeh, 58–69
Theureau, G., Bottinelli, L., Coudreau-Durand, N., et al. 1998, A&AS, 130, 333
Theureau, G., Hanski, M. O., Coudreau, N., Hallet, N., & Martin, J.-M. 2007, A&A, 465, 71
Thomas, R. C., Aldering, G., Antilogus, P., et al. 2011, ApJ, 743, 27
Vernet, J., Dekker, H., D'Odorico, S., et al. 2011, A&A, 536, A105
Whelan, J., & Iben, Jr., I. 1973, ApJ, 186, 1007
Zheng, W., & Filippenko, A. V. 2016, ArXiv e-prints, arXiv:1612.02097
Zheng, W., Kelly, P. L., & Filippenko, A. V. 2016, ArXiv e-prints, arXiv:1612.02725
Zheng, W., Silverman, J. M., Filippenko, A. V., et al. 2013, ApJL, 778, L15
Zheng, W., Shivvers, I., Filippenko, A. V., et al. 2014, ApJL, 783, L24